Optik xxx (2014) xxx–xxx

Contents lists available at ScienceDirect

Optik

journal homepage: www.elsevier.de/ijleo

Collection mode near-field scanning microwave microscopy

R. Cortés [a,*], V. Coello [a], R. Arriaga [b], N. Elizondo [b]

[a] CICESE, Monterrey, Km 9.5 Nueva carretera al Aeropuerto, PIIT, Apodaca Nuevo León, México
[b] UANL, FCFM, Doctorado en Ingeniería Física Industrial, Pedro de Alba S/N, San Nicolás de los Garza, Nuevo León, México

ARTICLE INFO

Article history:
Received 23 May 2013
Accepted 16 October 2013
Available online xxx

Keywords:
Scanning near field microwave microscopy
Dipole-like resonance
Dyadic Green's.

ABSTRACT

Collection mode near-field microscopy is demonstrated using a 10.56 GHz (X-band) frequency illumination. Imaging of a standing evanescent microwave was experimentally used to evaluate the capabilities of the microscope. The microscope functionality was validated by imaging near field interactions of different systems of dipole-like resonances. We prove that those microscope images contain near-field information by presenting numerical modeling of dipole-like resonant interactions. The model makes use of an analytic Dyadic Green's which is based in the near-field electrostatic approximation. We propose that this microscopy technique can be used, with certain limitations, as a check for 2D mapping of designed (spoof) surface plasmon at microwave frequencies.

1. Introduction

The first proposal for a super-resolution or subwavelength resolution microscope came from Synge in 1928 [1]. Four decades afterwards, in 1972, the experimental design was reported for the first time [2]. The experiment was carried out in the microwave range ($\lambda \approx 3$ cm), reaching a resolution of $\lambda/60$. Pohl and co-workers [3] showed the first optical version of this microscope, the so called scanning near-field optical microscope (SNOM). The success of the microscopy immediately inspired several operational modes [4]; nevertheless, the fundamental principles of the SNOM techniques are found in the detection of *evanescent waves* [5]. In this context, the collection mode [6] has become one of the most widely used SNOM versions. The reason is, at least partially, because of its high capability to study local optical field interactions. Such local fields contain information about the material or geometry of the object and the field may result from standard evanescent wave phenomena or more complicated processes including coupled electron-photon surface waves known as surface plasmon polaritons (SPPs) [7]. In collection-mode, the sample is illuminated by an extended field (from the top or bottom), as in classical microscopy, and the scattered near field is collected by a local probe. A particular case of collection mode SNOM is the photon scanning tunneling microscope (PSTM) [8,9]. The PSTM uses an uncoated fiber tip to probe the evanescent field of light being totally internally reflected at a sample surface. The tip is then brought into the extreme near field of the surface sample (≈10 nm) where the evanescent photons couple into the fiber-tip and are detected with a photon multiplier. Usage of SNOM techniques at microwave frequencies can provide several advantages and information complementary to optical imaging. For example, using a 3 cm microwave wavelength radically changes the scale of the experiment and therefore allows one a "scaling" of the optical problem under question. The scanning near field microwave microscopy (SNMM) has achieved resolutions in the scale of millimeter [2], micrometer [10], and even hundreds of nanometers [11,12]. Furthermore, SNMM has been applied in a diverse range of fields including biology [13], material science [14–17], and fundamental physics [18,19]. Even though in the microwave range, the mechanical and precision requirements are not as demanding as in the optical range, most of the SNMMs so far reported are not or at least until the best of our knowledge, of easy design and operation. In a previous work [20], we proposed a simple design for a scattering-type SNMM operating at a wavelength, $\lambda \approx 2.85$ cm (10.525 GHz, X-band). The device showed capabilities as a tool for testing potential two-dimensional optics devices [21–23]. In spite of this achievement, the microscope has the disadvantage of a strong far-field background signal that is typical of the scattering type near field microscopes [4,24]. As mentioned before, collection mode of the SNOM seems to be the most suitable technique for local and overall unobtrusive probing of near-field contributions. In this work, we report on the design and development of a versatile SNMM in collection (including tunnelling) mode. The capability of the microscope for mapping an evanescent mode was elucidated by imaging a standing evanescent wave. Furthermore, we validate our microscope functionality by imaging near field interactions of different systems of point-like dipoles. We prove that those microscope images contain near-field information by

* Corresponding author at: Unidad Monterrey, Centro de Investigación Científica y de Educación Superior de Ensenada, Alianza Centro 504, Autopista al Aeropuerto Km 10, CP 66629 Parque, PIIT, Apodaca, Nuevo León, Mexico. Tel.: +52 646 175 0500.
E-mail address: rcortes@cicese.mx (R. Cortés).

0030-4026/$ – see front matter © 2013 Elsevier GmbH. All rights reserved.
http://dx.doi.org/10.1016/j.ijleo.2013.10.085

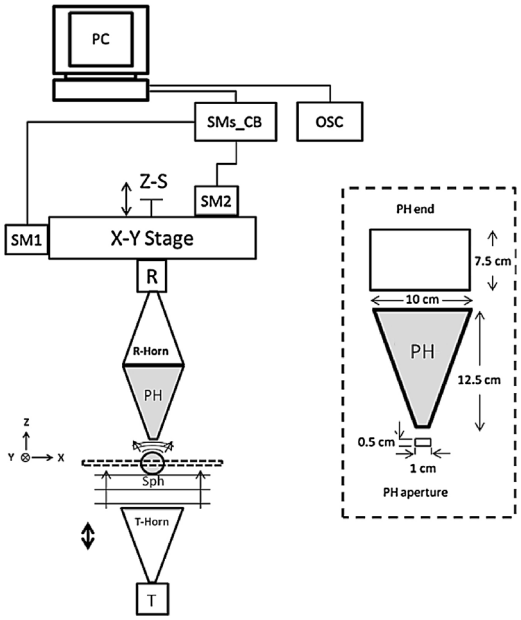

Fig. 1. Schematic of the experimental setup. T, Transmitter; R, Receptor; PH, Pyramidal Horn; Sph, Sphere; PC, Personal Computer. SMs_CB, Stepper Motors Controller Board; OSC, >Digital Oscilloscope; SM1, SM2, Step Motors 1 and 2; Z-S-Screw for z-motion.

presenting numerical modeling of dipole-like resonant interactions. The model makes use of an analytic Dyadic Green's which is based in the near-field electrostatic approximation.

2. Experimental setup

The experimental setup, as shown schematically in Fig. 1, consists of a collection mode SNMM using a (non-commercial) pyramidal waveguide horn as the collecting near-field probe. A pyramidal probe has already been proposed to improve throughput and light confinement in SNOM mechanisms [25]. The wide end of the pyramidal waveguide is attached to the microwave horn receiver whereas the narrow end is kept near the surface sample (Fig. 1). The probe is made of aluminum sheets and acts as a gradual transition from the collected/tunneled near-field modes to a free-space mode which is coupled to the horn receiver. The pyramidal probe has been filled with styrene pellets (n_{sp} = 1.35 at 10.525 GHz) in order to improve mode propagation efficiency inside of it. The resolution of the entire system is mainly determined by the size of the narrow end (Fig. 1). The microwave source is a commercial unit which consists of a Gunn diode microwave transmitter that provides 15 mW of coherent and linearly polarized microwave output at a wavelength, λ, of 2.85 cm. The microwave receiver is a microwave horn that is identical to that of the transmitter that collects the signal and channels it to a Schottky diode in a 10.525 GHz resonant cavity. The scanner is particularly simple in design and is based in a system of two stepper motors for motion control in the *xy* plane. The scanning is carried out in a stand-alone type, i.e., the probe is scanned along a fixed sample. A mechanical micrometrical screw is used for approach-retraction of the probe-sample distance. Once the probe is brought near the surface, the maximum level in the detected signal is taken as the probe-sample contact point. Finally, the signal is sent through a digital oscilloscope [26] and processed by a computer with the developed software that includes tools such as probe positioning in the *xy*-plane and speed scan regulation. The scan speed is basically limited by the number of collected data in every single mapped point. Typical collected values are 5000 sampled that ensure a sufficiently high signal-to-noise ratio in the detected signal. The resolution of the stepper motors has been fixed at 0.125 cm for every single step (pixel).

3. Theoretical Framework

3.1. Standing evanescent wave

The analysis of an interference pattern between two counterpropagating evanescent waves (standing evanescent wave) is generally accepted for calibration of a tunneling near-field microscope [27]. The intensity profile of the above mentioned standing evanescent wave is a square modulus of the superposition of the two evanescent waves, and it is given by the following expression

$$I(x,z) = I_0\, e^{-2K\sqrt{n^2\sin^2\theta - 1}\times z}\left[1+\rho^2+2\rho\cos\left(\frac{2\pi}{\Lambda}\times x\right)\right], \qquad (1)$$

where, we assume that the incident wave propagates along a (*x, z*) plane with z-axis being perpendicular to a surface plane. In Eq. (1), I_0 and θ are, respectively, the field intensity and the incidence angle of an illuminating plane; $K = 2\pi/\lambda_0$, with λ_0 being the light wavelength in vacuum, n is the refractive index of the prism, r is the reflection coefficient of the prism side face and $\Lambda = (\lambda_0/2n\sin\theta)$ is the period of modulation of the standing wave along the surface plane.

3.2. Dipole-like resonances

The local optical field of an illuminated object is of great interest and is often recorded with a collection mode SNOM. In this context, when an illuminated object is considerably smaller than the incident wavelength, the non-retarded approximation becomes applicable in order to model the possible near-field interactions. This approximation considers the small objects as dipoles or a set of dipoles whose susceptibilities may include dissipative effects. These assumptions lead to the construction of an approximate Green's tensor describing the near field terms produced by such dipoles. Thus, the self consistent field at the site of the dipoles in the process of multiple scattering takes the form [28]:

$$E(r_j) = E_0(r_i) + k_0^2\sum_{j\neq i}^{N} G\left(r_i, r_j\right)\times\alpha\times E(r_j), \qquad (2)$$

where, $E_0(r_i)$ is the self-consistent field at the site of scatterer-object i, k_0 is the wave vector of the incoming field in the space, $G(r_i,r_j)$ is the Green's tensor for near and far field regions (total field propagator), α is the polarizability of the scatterers. Here, the polarizability α has the surface dressing included i.e., the coupling of the dipole to itself through reflection in the surface. Furthermore, the polarizability, α, is a tensor describing the polarizability effect in each direction [27]:

$$\alpha = \left(I - k_0^2\frac{\alpha_0}{\varepsilon_0}\times G^S\left(r, r'\right)\right)^{-1}\times\alpha^0, \qquad (3)$$

where, α_0 is the free space polarizability tensor given as

$$\alpha^0 = \varepsilon_0 I 4\pi a^3\frac{\varepsilon-1}{\varepsilon+2}, \qquad (4)$$

with, I being the unit dyadic tensor, ε is the dielectric function (wavelength dependent), a is its radius and ε_0 is the vacuum permittivity. Equation (3) is valid when the long-wavelength electrostatic approximation has been used. Such approximation assumes that the field is constant within the considered range which corresponds to the size of the scatterer-object. For the approximation to be valid, the wavelength must be much bigger than the size of the scatterer. If the image dipole approximation is

Please cite this article in press as: R. Cortés, et al., Collection mode near-field scanning microwave microscopy, Optik - Int. J. Light Electron Opt. (2014), http://dx.doi.org/10.1016/j.ijleo.2013.10.085

Fig. 2. Gray-scale near-field images of $8 \times 6\,cm^2$ generated due to the standing evanescent wave at the surface on the base of the wax prism. The images were taken at the same place for different probe-to-surface distances: 0 (a), 2 .5 (b), and 10 mm (c).

used on $G^S(r,r')$ in Eq. (3), the following result is obtained for the polarizability tensor of Eq. (2).

$$\alpha \approx \left[\frac{\varepsilon-1}{\varepsilon+1} \times \frac{\varepsilon-1}{\varepsilon+2}\left(\frac{1}{8}\hat{x}\hat{x} + \frac{1}{8}\hat{y}\hat{y} + \frac{1}{4}\hat{z}\hat{z}\right)\right]^{-1} \times \alpha^0, \tag{5}$$

It should be mentioned that the dipole approximation assumes that the phase delay of the field, when it moves over the scatterer, is negligible. Mathematically, this means $e^{k\times r} \cong 1$ for a given field. This means again that the size of the scatterer should be smaller than the wavelength which is the main assumption in the model. When Eq. (5) has been used in Eq. (2) to determine the polarization, the final step is to calculate the field outside the scatterer-object as a self-consistent field:

$$E(r) = E^0(r) + k_0^2 \sum_i^N G(r, r_i) \times \alpha \times E(r_i), \tag{6}$$

considering both the source and observation points being close to a surface, one can propose to use a three-dimensional near-field electrostatic approximation of the total Dyadic Green's:

$$G_{nf}(r, r_s, \omega) = D_{nf}(r, r_s, \omega) + l_{ns}(r, r_s, \omega), \tag{7}$$

where, D_{nf} (r,r_s,ω) is the direct part of the near-field propagator given by

$$D_{nf}(r, r_s, \omega) = -\frac{c^2}{4\pi\omega^2}\frac{3e_R e_R - U}{R^2}, \tag{8}$$

with, r_s being the source point, $R = |r - r_s|$, $e_R = ((r - r_s)/R)$, and U being the unit tensor.

The indirect propagator has a complicated form and is usually expressed via its Fourier Transform [29]. However, in the non-retarded and local limit of the bulk response, the dipole-dipole interaction can be treated as a direct interaction between the dipole and its mirror image [30]. Thus, if the bulk surface coincides with the plane $z = 0$, $I_{nf}(r,r_s,\omega)$ can be expressed in the flowing form:

$$I_{nf}(r, r_s, \omega) = D_{nf}(r, r_{ms}, \omega) \times M(\omega), \tag{9}$$

where, r_{ms} points to the position of the mirror image of the source, and

$$M(\omega) = \frac{\varepsilon-1}{\varepsilon+1}\begin{pmatrix} -1 & 0 & 0 \\ 0 & -1 & 0 \\ 0 & 0 & 1 \end{pmatrix}, \tag{10}$$

the image dipole approach has been used to model physical mechanisms of the electromagnetic coupling between the probe tip and the sample in an SNOM configuration [31].

4. Results

We imaged a standing evanescent wave pattern that was created by directing the microwave beam perpendicular to a side face of a 90° wax prism and thereby obtaining the interference pattern related to the counterpropagating totally internally reflected waves with different amplitudes (Fig. 2(a)). Both, refractive index and reflectivity were experimentally obtained giving values of $n = 1.43$ and $r = 4\%$, respectively. In this case, the microscope was operated in tunneling mode. The microwave tunneling effect, trough an air gap, has been properly described in experiments with prisms made of dielectric pellets [32]. A high-frequency oscillation perpendicular to the direction of propagation (Fig. 2 (a)) was also observed. The oscillation is supposed to be stem from the electronic noise and/or mechanical vibrations of the scanner. Typically, those image artifacts appear as oscillations or repeating patterns in the image and they can be amended digitally as a posteriori by using image processing. If the probe-surface interaction is weak, the collected signal should replicate the total field existing in the absence of such probe, i.e., the probe would act as a passive detector [33]. In order to verify the near-field origin of the recorded image, we studied the dependence of the signal on the probe-surface distance. We observed that the evanescent field diminishes exponentially with distance from the interface (Fig. 2(a–c)). For example, the standing wave pattern was already hardly visible in a probe-to-surface distance of ~2.5 mm (Fig. 2. (b)) and then was practically independent in the distance (Fig. 2 (c)). Furthermore, the spatial period of the recorded interference pattern (Fig. 3) was rather close to the desirable value of $\Lambda = 1.42$ for prisms with the refractive index of ~1.43 as deduced from Eq. (1). We also have recorded in real space, and by purely collection SNMM means, near-field information of localized dipole-like resonances. In this context, we used a single steel sphere embedded in an ethafoam surface (Fig. 4(a)) which was uniformly illuminated with a plane microwave phase front. Thus, the steel sphere strongly interacts with microwaves while ethafoam is transparent to the microwaves. We found that a sphere of diameter ~1.75 cm produced (near-field) scattered signal amplitude large enough for detection and processing. For example, almost no signal could be obtained with a sphere of diameter less than 1 cm. In this context, near the detection limit of our microwave receiver, the signal-to-noise ratio was low, and therefore it was difficult to accurately measure the signal, leading to increased uncertainty of the detected signal. Once the appropriated sphere was placed, we observed that the field intensity distribution at the site of the probe, which was scanned in the (x, y) plane near the sphere ($z < 1$ mm), produced an object image in positive contrast (Fig. 4(b)). Based on Eq. (6), such near-field intensity distribution from a compact particle can be modelled as a sum of N point-dipoles located on a 3 mm-period square lattice. In our specific case, N was in the range

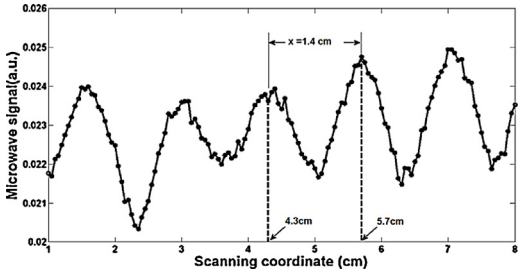

Fig. 3. Cross section of the standing evanescent wave shown in Fig. 2(a).

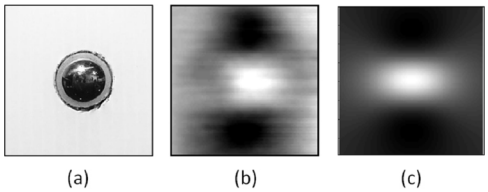

Fig. 4. Surface digital picture showing a sphere of diameter of 1.75 cm (a). Gray-scale near-field images (b) and calculation (c) of a point dipole-like resonance that was produced due to the interaction of the sphere with a plane microwave phase front.

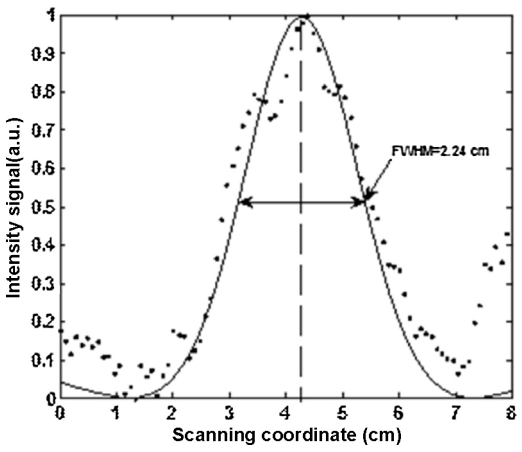

Fig. 5. Experimental (dotted curve) and numerical (solid curve) vertical cross section of the dipole-like resonances in Fig. 3(b, c) respectively.

of 110 to 115 and we found that the experimental data were best fitted in simulations if the diameter of the point dipoles was set to 1.45 mm (Fig. 4(c)). Hereafter, the entire systems are simulated for a dielectric constant $\mathring{a}_0 = 1$ and $\mathring{a} = 9$ [34], and the illumination conditions are kept the same for all the calculations. The calculated images show gray-scale representations of the distributions of the intensity $|E|^2$ for the illumination wavelength (2.8 cm). The total intensity field was calculated 80 nm above the spheres and, the incident beam has been removed i.e., only the scattered near-field appears in the pictures. Note that similar calculations have been done to model focusing and waveguiding of SPPs by using square-shaped nano-particles arrays [23]. For comparison, both calculated and measured cross sections of the intensity distribution along the illumination polarization direction are shown in Fig. 5. It was observed that the calculated and measured values of the peak signal amplitude as well as the FWHM were in reasonably good agreement (Fig. 5). If the resonance interaction becomes strong, as it could be in the case where nanoparticles are very close or even in physical contact with each other i.e., in the near-field domain [28,35], the total intensity field generated by such interaction is determined not only by the local surroundings but also by the large-scale geometrical structure. This feature is illustrated with the calculated and recorded total intensity field distributions obtained for a system composed of two identical spheres with an interparticle distance of $\sim\lambda/2$ (Fig. 5(a)). The results show a little correlation between these distributions and the dipole structure. In this case, the intensity field was distributed non-uniformly along the sphere chain (Fig. 5(b)); that is to say, the total field is different from that composed of distributions produced by an individual sphere as one may have expected. Qualitative comparison between numerical and experimental results showed a good correlation (Fig. 5(b,c)).

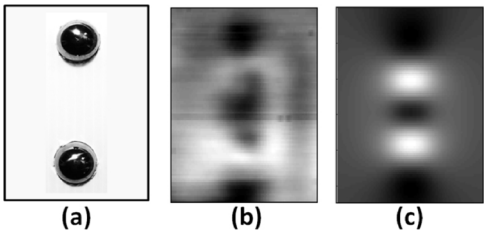

Fig. 6. Surface digital picture showing a system of two identical spheres of diameter of 1.75 cm (a). Gray-scale near-field images (b), and calculation (c) of the point dipole-like resonance that were produced due to the interaction of the sphere system with a plane microwave phase front.

5. Conclusions

We have designed and constructed a collection mode scanning near-field microwave microscope (SNMM), including electronics and software, and demonstrated that it works. The SNMM showed capabilities for imaging of evanescent microwaves. The nature of the detected signal was confirmed by sample-to-probe distance dependent on a generated standing wave interference pattern. The observed oscillation perpendicular to the direction of propagation may have its origin in the electronic noise and/or mechanical vibrations of the scanner. Experimental results obtained for dipole-like resonances have been presented. In this context, a single and a double system of dipoles were artificially fabricated by placing metal spheres in an ethafoam surface. The single sphere showed an object image in positive contrast whereas the image of two-dipoles system was mainly determined by the large scale geometrical structure instead of the local surroundings. Numerical simulations based on the Green's tensor formalism showed a good match with the experimental results Fig. 6. The numerical calculations were carried out by using a relatively simple vectorial dipolar model for multiple scattering that allows one to explicitly formulate the set of linear equations for the self-consistent field, facilitating greatly computer aided design considerations. We also conclude that this microscopy technique can be employed, by incorporating a broad band microwave source, as a check for 2D mapping of designed (spoof) Surface Plasmon [36] which is the newly discovered ability to confine, guide, and manipulate microwaves in subwavelength open structures. We are conducting further investigations in this area.

Acknowledgment

The authors acknowledge financial support from CONACyT project 127589 and scholarship 28959.

References

[1] E.H. Synge, A suggested method for extending microscopic resolution into the ultra-microscopic region, Phil. Mag. 6 (1928) 356–362.
[2] E. Ash, G. Nicholls, Super-resolution aperture scanning microscope, Nature 237 (1972) 510–512.
[3] D.W. Phol, W. Denk, M. Lanz, Optical stethoscopy: Image recording with resolution λ/20, Appl. Phys. Lett. 44 (1984) 651–653.
[4] D.W. Pohl, D. Courjon, Near Field Optics, Kluwer, The Netherlands, 1993.
[5] F. de Fornel, Evanescent Waves: from Newtonian Optics to Atomic Optics, Springer, Berlin, 2001.
[6] E. Betzig, M. Isaacson, A. Lewis, Collection mode near-field scanning optical microscopy, Appl. Phys. Lett. 51 (1987) 2088–2090.
[7] H. Raether, Surface Plasmons, Springer Tracts in Modern Physics, 111, Springer, Berlin, 1988.
[8] N.F. van Hulst, F.B. Segerink, F. Achten, B. Bolger, Evanescent-field optical microscopy: effects of polarization, tip shape and radiative waves, Ultramicroscopy 42 (1992) 416–421.
[9] T.L. Ferrell, J.P. Goudonnet, R.C. Reddick, S.L. Sharp, R.J. Warmack, The photon scanning tunneling microscope, J. Vac. Sci. Technol. B 9 (1991) 525–530.
[10] C. Gao, T. Wei, F. Duewer, Y. Lu, X.D. Xiang, High spatial resolution quantitative microwave impedance microscopy by a scanning tip microwave near-field microscope, Appl. Phys. Lett. 71 (1997) 1872–1874.
[11] Tabib-Azar, D. Su, A. Pohar, S.R. LeClair, G. Ponchak, 0.4 μm spatial resolution with 1 GHz (λ = 30 cm) evanescent microwave probe, Rev. Sci. Instrum. 70 (1999) 1725–1729.
[12] L. Zhang, Y. Ju, A. Hosoi, A. Fujimoto, Microwave atomic force microscopy imaging for nanometer-scale electrical property characterization, Rev. Sci. Instrum. 81 (2010) 123708–123712.
[13] J. Park, S. Hyun, A. Kim, T. Kim, K. Char, Observation of biological samples using a scanning microwave microscope, Ultramicroscopy 102 (2005) 101–106.
[14] N. Okazaki, H. Odagawa, Y. Cho, T. Nagamura, D. Komiyama, T. Koida, H. Minami, P. Ahmet, T. Fukumura, Y. Matsumoto, M. Kawasaki, T. Chikyow, H. Koinuma, T. Hasegawa, Development of scanning microwave microscope with a lumped-constant resonator probe for high-throughput characterization of combinatorial dielectric materials, Appl. Surf. Sci. 189 (2002) 222–226.
[15] A. Imtiaz, T. Baldwin, H.T. Nembach, T.M. Wallis, P. Kabos, Near-field microwave microscope measurements to characterize bulk material properties, Appl. Phys. Lett. 90 (2007) 243105–243107.

Please cite this article in press as: R. Cortés, et al., Collection mode near-field scanning microwave microscopy, Optik - Int. J. Light Electron Opt. (2014), http://dx.doi.org/10.1016/j.ijleo.2013.10.085

[16] W. Kundhikanjana, K. Lai, M.A. Kelly, Z. Shen, Cryogenic microwave imaging of metal–insulator transition in doped silicon, Rev. Sci. Instrum. 82 (2011) 033705–033709.
[17] J.C. Weber, J.B. Schlager, N.A. Sanford, A. Imtiaz, T.M. Wallis, L.M. Mansfield, K.J. Coakley, K.A. Bertness, P. Kabos, V.M. Bright, A near-field scanning microwave microscope for characterization of inhomogeneous photovoltaics, Rev. Sci. Intrsum. 83 (2012) 083702–083708.
[18] A. Imtiaz, M. Pollak, S.M. Anlage, J.D. Barry, J. Melngailis, Near-field microwave microscopy on nanometer length scales, J. Appl. Phys. 97 (2005) 044302–044307.
[19] S. Kim, Y. Jang, S. Kim, T.D. Kim, H. Melikyan, A. Babajanyan, K. Lee, B. Friedman, Detection of DNA-hybridization using a near-field scanning microwave microscope, J. Nanosci. Nanotechnol. 11 (2011) 4222–4226.
[20] V. Coello, R. Villagomez, R. Cortes, R. Lopez, C. Martinez, Near-field microscopy of evanescent microwaves, Rev. Mex. Fis. 51 (2005) 426–430.
[21] S.I. Bozhevolnyi, V. Coello, Elastic scattering of surface plasmon polaritons: modeling and experiment, Phys. Rev. B. 58 (1998) 10899–10910.
[22] H. Ditlbacher, J.R. Krenn, G. Schider, A. Leitner, F.R. Aussenegg, Two-dimensional optics with surface plasmon polaritons, Appl. Phys. Lett. 81 (2002) 1762–1764.
[23] I.P. Radko, A.B. Evlyukhin, A. Boltasseva, S.I. Bozhevolnyi, Refracting surface plasmon polaritons with nanoparticle arrays, Opt. Exp. 16 (2008) 3924–3930.
[24] F. Keilmann, Scattering-type near-field optical microscopy, J. Electron. Microsc. 53 (2004) 187–192.
[25] X.Q. Wang, S.F. Wu, G.S. Jian, S. Pan, The advantages of a pyramidal probe tip entirely coated with a thin metal film for SNOM, Phys. Lett. A 319 (2003) 514–517.
[26] Tektronik, Digital Posphor Oscilloscope, TDS3000B Series.
[27] A.J. Meixner, M.A. Bopp, G. Tarrach, Direct measurement of standing evanescent waves with a photon-scanning tunneling microscope, Appl. Opt. 33 (1994) 7995–8000.
[28] T. Søndergaard, S.I. Bozhevolnyi, Vectorial model for multiple scattering by surface nanoparticles via surface polariton-to-polariton interactions, Phys. Rev. B. 67 (2003) 165405.
[29] C. Girard, A. Dereux, O.J.F. Martin, M. Devel, Generation of optical standing waves around mesoscopic surface structures: scattering and light confinement, Phys. Rev. B. 52 (1995) 2889–2898.
[30] O. Keller, M. Xiao, S.I. Bozhevolnyi, Configurational resonances in optical near-field microscopy: a rigorous point-dipole approach, Surf. Sci. 280 (1993) 217–230.
[31] C. Wu, M. Ye, H. Ye, Image dipole approach and polarization effects in scanning near-field microscopy, Optik 116 (2005) 277.
[32] F. Albiol, S. Navas, M.V. Andres, Microwave experiments on electromagnetics evanescent waves and tunneling effect, Am. J. Phys. 61 (1993) 165.
[33] R. Carminati, J.-J. Greffet, Two-dimensional numerical simulation of the photon scanning tunneling microscope: concept of transfer function, Opt. Commun. 116 (1995) 316–321.
[34] M. Hotta, M. Hayashi, M.T. Langan, D.K. Agrawal, K. Nagata, Complex permittivity of graphite, carbon black and coal powders in the ranges of X-band frequencies (8.2 to 12.4 GHz) and between 1 and 10 GHz, ISIJ Int. 51 (2011) 1766–1772, http://www.rfcafe.com/references/electrical/dielectric-constants-strengths.htm.
[35] P. Segovia, V. Coello, Elastic surface plasmon polariton scattering: near- and far- field interactions, NANO 7 (2012) 1150003, 2012.
[36] A.P. Hibbins, E. Hendry, M.J. Lockyear, J.R. Sambles, Prism coupling to 'designer' surface plasmons, Opt. Express 16 (2008) 20441–20447.

Please cite this article in press as: R. Cortés, et al., Collection mode near-field scanning microwave microscopy, Optik - Int. J. Light Electron Opt. (2014), http://dx.doi.org/10.1016/j.ijleo.2013.10.085